Production and Study of Triply Charged Diatomic Ions with Femtosecond Pulses: Application to Cl_2^{3+}†

R. J. Verver, D. R. Matusek, and J. S. Wright*

Department of Chemistry, Carleton University, 1125 Colonel By Dr., Ottawa, Canada K1S 5B6

G. N. Gibson

Department of Physics, University of Connecticut, Storrs, Connecticut 06269

R. Bhardwaj, S. Aseyev, D. M. Villeneuve, P. B. Corkum, and M. Yu. Ivanov

Steacie Institute for Molecular Sciences, National Research Council of Canada, 100 Sussex Drive, Ottawa, Ontario K1A 0R6, Canada

Received: October 24, 2000; In Final Form: January 17, 2001

We describe the preparation of diatomic trications using intense femtosecond laser pulses, and discuss the feasibility of using femtoseond pump−probe techniques to measure the vibrational spectrum of Cl_2^{3+}. Initial attempts to observe the vibrational spectra of Cl_2^{3+} were unsuccessful. Possible refinements to the experiment are guided by calculations of the electronic states, transition moments, and field-dressed potential curves for Cl_2^{3+}. Solution of the time-dependent Schrödinger equation using these theoretical data as input allow an accurate simulation of pump−probe experiments and their time-delay signals. Optimization of the experimental parameters via the simulation suggests an improved approach to obtaining the spectra of trications, with special emphasis on the unusual aspects of these systems.

1. Introduction

Modern femtosecond pulses allow one to create electric fields comparable to, or even exceeding those which bind electrons in atoms and in molecules. Combined with less than 10 fs time resolution (presently about 5 fs), these pulses offer unique opportunities in many areas of laser-matter interaction. In molecular reaction dynamics, they bring about the ability to time-resolve nuclear motion,[1] strongly modify potential energy surfaces, and remove several electrons while the nuclei remain stationary. Applications include time-resolved femtochemistry, laser-induced Coulomb explosion imaging, and control of molecular reaction dynamics.

One of the unusual properties of intense ultrashort infrared pulses is their ability to efficiently create highly charged molecular ions, such as triply charged ions of diatomic molecules. A general feature of small highly charged species such as diatomic trications is that "the majority of the diatomic trications do indeed exhibit entirely repulsive potential energy curves".[2] In the more unusual case when metastable states are present, the efficiency of the production of trications depends on the ability of femtosecond pulses to (i) quickly remove three electrons from the neutral species before the nuclei undergo any significant motion and (ii) avoid strong excitation of the remaining electrons. These species are quite fragile, with metastable minima on the ground state potential energy surface only a fraction of an eV deep and frequently no other metastable electronic states.

Quick removal of electrons is accomplished by using sufficiently short pulses, whereas avoiding strong excitation results from applying intense infrared fields which bring multiphoton ionization into the tunneling regime. In this regime electrons are removed adiabatically sequentially, and multielectron excitation is minimal. In the tunneling regime the molecule is typically produced on the lowest potential energy surface shifted and modified by the AC Stark shift (the "dressed surface"). Electronic excitation appears in the limit of ultrashort pulses: as the field is quickly turned off, dressed surfaces change in time, causing nonadiabatic Landau−Zener-type transitions.

A survey of the existence of metastable diatomic trications that have been studied experimentally was given by Schröder and Schwarz,[2] and as of 1999 the list includes only VHe^{3+}, SF^{3+}, TiF^{3+}, VO^{3+}, VF^{3+}, UF^{3+}, CS^{3+}, and S_2^{3+}, and the halogens Cl_2^{3+}, Br_2^{3+}, and I_2^{3+}. Diatomic trications that have only a single metastable electronic surface present a challenge for optical spectroscopy, since electronic excitation spectra to repulsive states are diffuse and not definitive. To the best of our knowledge, the only experimental evidence for such species to date has been their mass spectra, although a few theoretical calculations have reported the position and depth of the potential minimum.[2] Clearly, it would be of great interest to measure the vibrational spectra of diatomics containing +3 or higher charge.

In a previous study[12] we proposed the use of strong-field femtosecond Raman spectroscopy to determine trication vibrational frequencies. In that work, time-of-flight (TOF) mass spectra were shown which were evidence for formation of all three of the halogen trications Cl_2^{3+}, Br_2^{3+}, and I_2^{3+}. Isotopic data were also consistent with expected abundances to within ca. 20%. The importance of pulse duration for pump and probe pulses was also discussed, concluding that, for Cl_2^{3+}, pulses

† Part of the special issue "Aron Kuppermann Festschrift". Dedicated to Professor Aron Kuppermann on the occasion of his 65th birthday.

10.1021/jp003914g CCC: $20.00
Published on Web 02/24/2001

with intensity of $\sim 10^{14}$ W/cm^2 led to complete dissociation of bound states for pulses of 100 fs duration or longer. It was also suggested theoretically that by using strong-field Raman spectroscopy it should be possible to observe modulation in the signal representing the total amount of trications reaching the detector, as a function of the frequency difference $\Delta\omega$ between the two simultaneous femtosecond pulses. Specifically, our calculations supported the natural expectation that when $\Delta\omega = \omega_1 - \omega_2 \sim E(v = 1) - E(v = 0)$, the $v = 0$ state should be significantly depleted. It was proposed to detect this $\Delta\omega$-dependent population transfer and dissociation. This approach, however, is experimentally very difficult: due to uncertainty in the initial vibrational states of Cl_2^{3+} it required a complicated arrangement of four probe pulses. Here, we investigate alternative methods to obtain the vibrational spectrum.

Femtosecond pulses used to efficiently produce trications can also be used for measurement of their vibrational spectra. However, the need to use very intense pulses (up to $I \sim 10^{15}$W/cm^2) to create trications introduces several novel aspects into standard techniques of femtosecond pump−probe spectroscopy and places important requirements on both the pump and the probe. We discuss various approaches to pump−probe spectroscopy, and illustrate them with numerical simulations. Our initial pump−probe experiment designed to measure the vibrational spectrum of Cl_2^{3+} did not produce any definitive result. On the basis of the experimental observations, we explore various constraints on the pump and probe pulses and illustrate the importance of the theoretically determined requirements.

The paper is organized as follows: section II presents a theoretical framework for calculation of their vibrational spectra, using Cl_2^{3+} as an example. Section III describes an experimental setup for the production of trications. Section IV shows (preliminary) experimental data on Cl_2^{3+}, followed by calculations on the electronic structure and transition moments of Cl_2^{3+}. Field-dressed potential curves are given for typical laser field strengths, and the time-dependent Schrödinger equation is solved to obtain a simulation of the experiment. Section V discusses the interrelationship between the experimental parameters and the theoretical prediction of the vibrational spectra and explores the parameter space with additional numerical simulations. We conclude with a set of general observations on the feasibility, novel aspects, and requirements for the femtosecond pump−probe spectroscopy of trications.

2. Theoretical Methods

2.1. Electronic States. Calculations of the potential energy curves for diatomic chlorine (Cl_2) have been reported by Peyerimhoff and Buenker,[3] and for the higher charged ions by some of the present authors.[4] Of interest to the present study are the $X^1\Sigma_g^+$ ground state of Cl_2, the $X^2\Pi_g$ metastable ground state and a selection of excited states of the trication Cl_2^{3+}. As will be seen, an accurate treatment of the relevant states and the transitions between them is required for any comparison to experiment, so the calculations will be extended in this paper beyond those reported in ref 4.

The MRD-CI method of Buenker and co-workers[5] was used to generate the relevant electronic states for Cl_2 and Cl_2^{3+}. Details of the method as applied to Cl_2 and its ions Cl_2^{n+} (n = 1, 2, 3, 4, 6, 8, 10) were discussed in our study of the deviation from Coulombic behavior in Coulomb explosions of Cl_2.[4] Briefly, the MRD-CI method is a multireference (MR) configuration interaction (CI) method, where the multireference starting point is necessary to give the proper dissociation properties along the potential curve. It is also important in obtaining an accurate barrier height for metastable states. We used the same set of contracted functions described in ref 4, consisting of an atomic 10s7p2d basis set, along with additional s,p functions located at the bond midpoint to describe polarization effects. Molecular orbitals of appropriate spin and symmetry were generated from this basis set for a given molecular electronic state. Electrons in the inner-shell orbitals (corresponding to Ne in the atomic limit) were frozen and their high-lying complementary MO's were discarded, leaving 70 MO's available for the CI calculation. A reference set of ca. 40 symmetry-adapted functions (SAF's, also termed configurations) was chosen (see below), and all single and double-excitations from the reference set were used to generate the total MRD-CI space, of order 10^6 SAF's. The desired number of n roots (excited states) of a given symmetry was chosen, and a subset of the total SAF space determined according to its ability to interact with the reference set and lower the total energy of any of the n roots, which depends on the choice of a selection threshold (typically 3−4 μhartree in this work). An extrapolation procedure was used to estimate the MRD-CI energy at zero selection threshold followed by the multireference Davidson correction to give the estimated full-CI energy, which then becomes a point on the potential energy curve for the relevant state(s). These potential energy data were spline-fitted, and the Numerov−Cooley procedure was used to obtain the bound vibrational levels.[6]

2.2. Transition Moments. Nonzero transition moments in Cl_2^{3+} arise between the ground state $X^2\Pi_g$ and the two excited states $^2\Pi_u$ and $^2\Sigma_u^+$. For $^2\Pi_g \rightarrow {}^2\Pi_u$ transitions, the transition moment μ_{ij} has a nonzero component parallel (μ_{zz}) to the internuclear axis. For $^2\Pi_g \rightarrow {}^2\Sigma_u^+$ transitions, transition moments are nonzero for perpendicular transitions (μ_{xx} and μ_{yy}). The energies of these electronic states and the transition moments between them enter into the field-dressed equations, which are of special importance when a resonant transition can occur.

The potential energy surfaces and transition dipole matrix elements are shown in Figure 1 and Figure 2 respectively; discussion of the results is presented in section IV.

2.3. Field-Dressed Potential Curves. Although our numerical model does not use the rotating wave approximation (RWA),[7] the dressed-state picture that is obtained in this approximation provides useful qualitative guidelines in understanding the dynamics of Cl_2^{3+}. For the ground state, the largest dipole coupling is to the state $1^2\Pi_u$. This coupling is also one-photon resonant near the point of vertical transition from the neutral molecule. The Hamiltonian matrix for the field-dressed 2-state system in atomic units and the RWA has elements $H_{11} = E_1$, $H_{22} = E_2 - \omega_L$, $H_{12} = H_{21} = (1/2)\mu_{12}\epsilon_0$, where 1 = ground state $X^2\Pi_g$, 2 = excited state $1^2\Pi_u$, ϵ_0 is the electric field strength, μ_{12} is the transition moment between the two states, and the $1^2\Pi_u$ state was lowered by the photon energy ω_L corresponding to a laser wavelength of 800 nm.

2.4. Wave Packet Dynamics. For the wave packet dynamics, the vibrational wave packet is propagated on coupled potential energy surfaces. The time-dependent Schrödinger equation for the coupled-state problem is (in au)

$$i\frac{\partial}{\partial t}\vec{\chi}(R,t) = \hat{H}\vec{\chi}(R,t) \qquad (1)$$

where $\vec{\chi}(R,t)$ is the column vector of vibrational wave functions for the potential energy surfaces of interest, the diagonal elements of $\hat{H}$ describe the motion on the corresponding

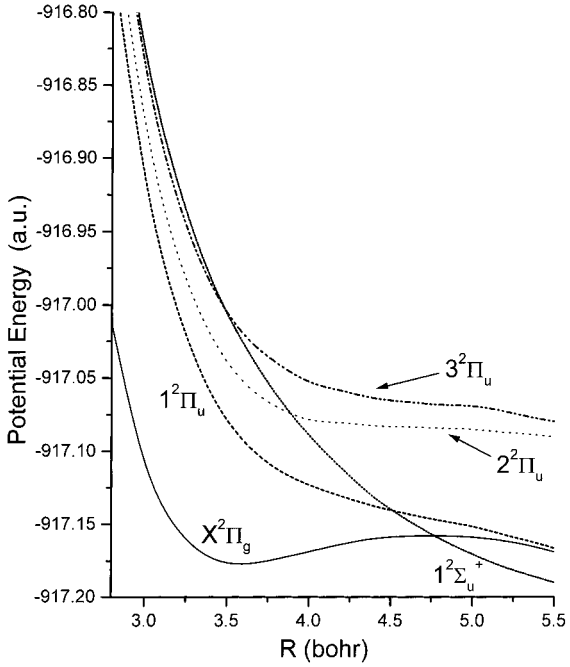

Figure 1. Potential curves for the ground and low-lying excited states of Cl_2^{3+}.

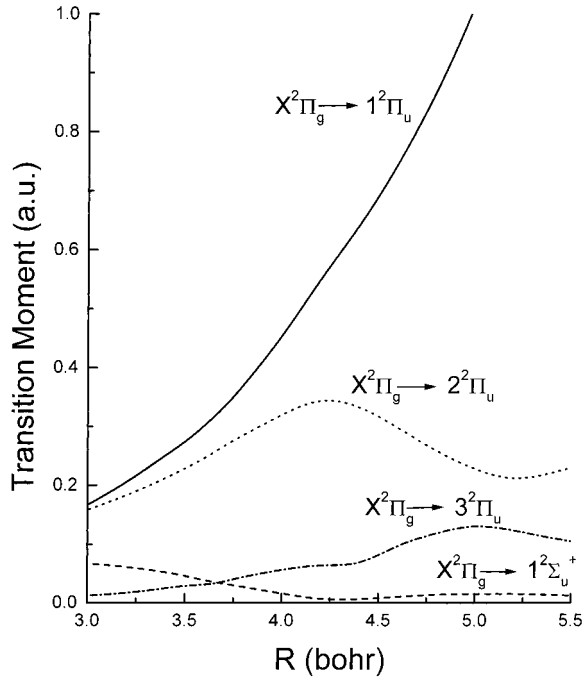

Figure 2. Transition dipole moment curves for the ground and low-lying excited states of Cl_2^{3+}.

potential energy surface $|i\rangle$, $\hat{H}_{ii} = \hat{P}^2/2\mu + E_i(R)$, and off-diagonal elements describe the dipole coupling, $H_{ij} = \mu_{ij}\epsilon_0 f(t) \cos(\omega_L t + \sigma_L)$, where μ_{ij} is the transition moment between the two electronic surfaces. Here μ is the reduced mass of Cl_2, $f(t)$ is the laser envelope, and ϕ_L is the initial phase of the pulse. In most cases, the neutral chlorine ground state ($v = 0$) is sent vertically to the $X^2\Pi_g$ ground state, where it is then coupled to the $1^2\Pi_u$ excited state by the laser field. Other initial conditions for Cl_2^{3+} are also studied.

Surfaces $E_i(R)$ and the initial wave packet are read in as discrete data and fitted with natural cubic splines. Next, the time is specified when the pump pulse is initiated (field-free evolution of the wave packet can be studied when there is no pump pulse present). Characteristics of the pump pulse are described, including the maximum field strength ϵ_0, the laser frequency ω_L, the laser phase ϕ_L, the zero-to-zero length of the pump pulse, and the pulse shape $f(t)$ (usually a $\sin^2$ shape). The above data are repeated for each probe pulse, and a T_{off} is chosen, the field-free delay time between the pump pulse and the probe pulse. After all probe pulses have been described, T_{free} is input, which describes how long the wave packet is allowed to evolve after the last probe pulse, and Δt, the time step for the numerical integration. The numerical integration uses the standard split operator method, with a smooth masking function that absorbs the wave packet at large R. In the present case we used an s-type masking curve centered at 19 bohr and decreasing to zero in a range of 2 bohr.

3. Experimental Method

The laser system consists of a mode-locked Ti:sapphire oscillator whose output is regeneratively amplified at a repetition rate of 310 Hz to a maximum pulse energy of 500 μJ. To obtain short (12 fs), high-energy pulses,[8] the 50 fs pulses from the regenerative amplifier were focused into a 50 cm long hollow core fiber (250 μm inner diameter) filled with Ar at 1 atm. The spectrum was broadened to $\sim$200 nm fwhm by self-phase modulation. Pulse chirp was removed by two pairs of fused silica prisms (20° apex angle) in double pass geometry to achieve a pulse duration of 12 fs and maximum pulse energy of 100 μJ.

Either the 50 fs or the 12 fs pulses were focused by a 5 cm on-axis parabolic mirror placed in a high vacuum chamber with a base pressure of 10^{-8} Torr. A magnified image of the focal spot of both the pulses shows a 1.7 times diffraction limited focus. We estimate the focal spot diameter inside the vacuum chamber to be 6 and 5.4 μm fwhm for 50 and 12 fs pulses, respectively. Typical laser intensities were $1-10 \times 10^{14}$ W/cm^2.

Chlorine gas was leaked through a jet into the vacuum chamber at $\sim 10^{-7}$ Torr. The ions were analyzed by a time-of-flight spectrometer described in detail elsewhere.[9] The time-of-flight (TOF) chamber had its TOF axis oriented perpendicularly to the jet axis and to the direction of propagation of the laser beam. The molecular ions passed through an accelerating region and a field-free drift region, reaching a microchannel plate detector in about 1 μs.

The microchannel plate (MCP) detector was operated in ion-counting mode in conjunction with a multichannel scaler. We obtained ion yields by integrating the appropriate peaks. We used a half-wave plate and a polarizer to vary the intensity of 50 and 12 fs pulses. For the 50 fs pulses, both of them were used before the grating compressor. To accommodate the broad bandwidth of a 12 fs pulse, we used a half-wave plate before the hollow core fiber to rotate the polarization. This does not change the energy or the pulse duration. Since the system is axially symmetric, self-phase modulation is not affected and the polarization remains linear. We used a germanium slab at Brewster's angle to reflect only the "s" component of the polarization after the fiber.

A broad-bandwidth 12 fs pulse is extremely sensitive to dispersion. To obtain minimum pulse width in the vacuum chamber we must compensate for the dispersion of air and vacuum chamber (6 mm) fused silica windows. Since below the saturation intensity, Cl_2^{3+} yield is very sensitive to peak intensity and hence pulse duration, at an intensity of (2×10^{15} W/cm^2, we maximized the Cl_2^{3+} signal by changing the prism position. After passing through the equivalent amount of air and material of the beam splitter and vacuum chamber windows,

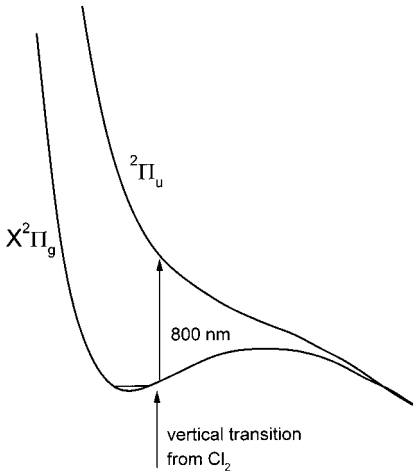

Figure 3. Schematic ground- and excited-state potential curves for Cl_2^{3+} showing the position of the initial wave packet and the position of the resonance.

we also measured the pulse duration to be 12 fs by second harmonic frequency resolvet optical Gating (FROG) technique using a 10 μm BBO crystal.

As shown in Figure 3, if the pump pulse induces a vertical transition from the ground vibrational state of a neutral molecule to the ground state of Cl_2^{3+}, a wave packet is launched near the right turning point. This is also the region where one-photon resonance between the ground state $X^2\Pi_g$ and the excited state $1^2\Pi_u$ occurs at a laser wavelength of $\lambda = 800$ nm. Each time the wave packet approaches its right turning point, 800 nm light should induce efficient dissociation. Then a probe pulse, with the duration shorter than the vibrational period of Cl_2^{3+}, should produce modulation in the total number of detected Cl_2^{3+} ions as a function of the delay between the pump and the probe.

For the pump−probe measurements, we used linearly polarized, short pulses (12 fs) from the hollow-core fiber. A thin polarizing beam splitter was used to divide the beam into the two arms of a Michelson interferometer to generate pump and probe pulses at desired delays. A half-waveplate was used before the beam splitter to control the relative intensities of the pump and probe. A compensating glass plate was used in one of the arms to equalize the pulse duration of pump and probe. The polarizations of pump and probe pulses were circular, to exclude preference of ionization along the molecular axis. Circular polarization was introduced by a quarter waveplate placed after the beam splitter.

The pulse durations of both pump and probe were optimized by maximizing the Cl_2^{3+} signal by changing the prism position after the fiber. The signal intensity corresponding to the number of Cl_2^{3+} ions reaching the detector was recorded as a function of the time delay. Ideally, this signal contains the data from which one could recover the vibrational spectrum.

4. Results and Discussion

4.1. Experimental Data on Cl_2^{3+}. Figure 4 shows the yield of triply charged ions Cl_2^{3+} as a function of laser intensity, for two pump pulses of duration 12 and 50 fs (for comparison, the vibrational period of Cl_2^{3+} is ~70 fs). These ions are necessarily stable within the time to reach the detector, $\sim 10^{-6}$ s. It is clear that the production efficiency increases significantly for shorter pulses. For pulses longer than the vibrational period of Cl_2^{3+}, the efficiency drops quickly.[12] The reason for this is that, at the high intensities needed for the production of Cl_2^{3+}, its

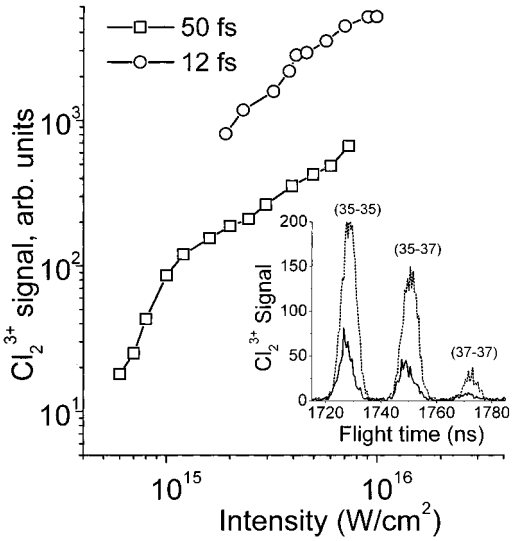

Figure 4. Yield of Cl_2^{3+} for two pump pulse durations. (Circles) 12 fs pulse, (squares) 50 fs pulse. Inset: time-of-flight mass spectrum of Cl_2^{3+}. (Solid curve) 50 fs pulse, (dashed curve) 12 fs pulse.

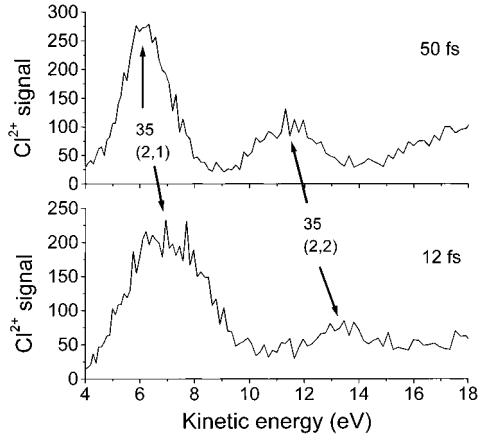

Figure 5. Kinetic energy spectrum of fragments created during the Coulomb explosion of Cl_2^{3+} and Cl_2^{4+}, for 50 fs (a) and 12 fs (b) pulses. For shorter pulses (i) positions of the peaks shift toward the Coulomb energy of explosion from the equilibrium position of the neutral, and (ii) peaks are significantly broader.

field-free electronic structure is very strongly modified and the ground-state becomes dissociative due to bond-softening at intensities $I \sim 10^{13}$ W/cm^2 and above (Figure 6). Transient trapping in the laser-induced well on the excited surface is only possible while the field is on (see also Figure 6). Slow turn-off leads to gradual disappearance of the laser-induced well and consequent dissociation, which can only be avoided with short pulses.

The efficiency of the production of trications can be estimated by comparing it with the production of singly- and doubly charged molecular ions, which are also simultaneously produced. Taking into account the efficiency of the detector for different charge states, at an intensity of 3×10^{15} W/cm^2, the estimated ratios of Cl_2^+ to Cl_2^{2+} and Cl_2^+ to Cl_2^{3+} are roughly 6 and 500 respectively, for the pulse duration of 12 fs.

If Cl_2^{3+} dissociates after the end of the pulse, the corresponding atomic fragments are Cl_2^{2+} and Cl_2^+. During the Coulomb explosion, the fragments are ejected both in the forward and the backward direction along the time-of-flight axis. Figure 5 shows energy spectra of Cl^{2+} fragments ejected in the backward direction.

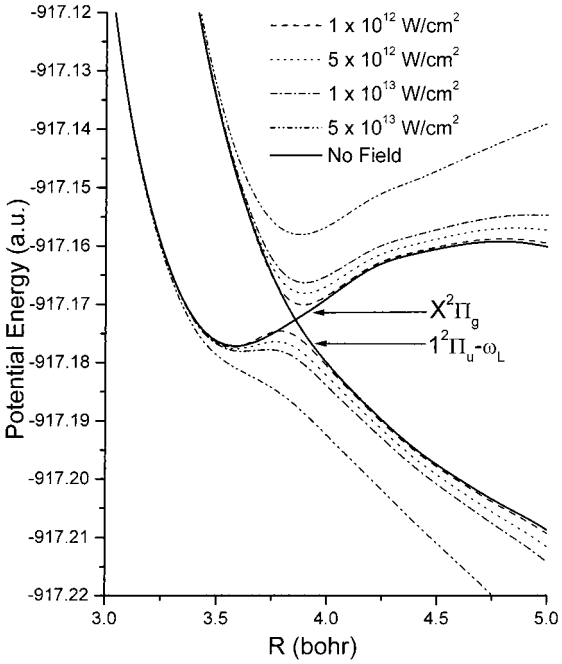

Figure 6. Potential energy surfaces in Cl_2^{3+} with and without resonant laser field.

There are important differences in mass spectra obtained with 12 and 50 fs pulses. First, there is a significant increase in the kinetic energy of all fragmentation channels. While for 50 fs pulses the characteristic energy is less than the corresponding energy of Coulomb explosion from the equilibrium distance of the neutral parent, for 12 fs pulses peaks in the spectrum have energy very close to that of the Coulomb explosion from the equilibrium distance. Hence, for 12 fs pulses excitation from neutral chlorine to Cl_2^{3+} is vertical. Since the equilibrium distance for Cl_2^{3+} is less than that for neutral Cl_2,[4] vibrational excitation should be expected.

Second, for 12 fs pulses Figure 5 shows that peaks corresponding to fragmentation of Cl_2^{3+} into Cl^{2+} and Cl^+ are clearly broader than those for 50 fs pulses by several eV, as well as peaks in other fragmentation channels. Such energy blurring for all fragmentation channels is to be expected and is consistent with a higher probability of electronic and vibrational excitation due to rapid changes of dressed potential energy surfaces in short pulses. Strong excitation in this limit is unavoidable.

To summarize the experimental results, our data show that (i) intense ultrashort pulses of infrared laser radiation can be used to efficiently remove several electrons and produce metastable Cl_2^{3+}; (ii) for 12 fs pulses, the transition $Cl_2 \rightarrow Cl_2^{3+}$ is vertical or nearly vertical and vibrational excitation is expected; (iii) electronic excitation of Cl_2^{3+} in 12 fs is more significant than in 50 fs pulses; and (iv) electronic excitation is also more probable in other charge states, both higher and lower.

4.2. Potential Energy Curves. The calculated properties of the $X^2\Pi_g$ ground state are shown in Table 2, where R_e is the position of the potential minimum, R_{max} the position of the maximum, and D_{eff} is the well depth (measured from the minimum). Good consistency was obtained between this and the earlier calculations, which differed, for example, by only 2 cm^{-1} in the $v = 0 \rightarrow 1$ frequency. Thus, the treatment is stable with respect to the CI calculation, although there could still be some additional changes resulting from further enlargement of the basis set.

TABLE 1: Technical Details of the MRD-CI Calculation[a]

species	state	no. of mains	no. of roots	threshold (μhartree)	total SAFs	selected SAFs
Cl_2	$^1\Sigma_g^+$	38	4	4	1 358 851	16000-31000
Cl_2^{3+}	$^2\Pi_g$	40	3	3	2 110 409	16000-23000
Cl_2^{3+}	$^2\Pi_u$	24	3	3	1 332 684	15000-22000
Cl_2^{3+}	$^1\Sigma_u^+$	63	3	3	2 737 589	14000-23000

[a] Notation: main = reference configuration, SAF = symmetry-adapted function (configuration), threshold = energy selection threshold for CI selection procedure.

TABLE 2: Comparison of Properties Derived from Potential Energy Curves for $X^2\Pi_g$ State of Cl_2^{3+} between Those Obtained from a Smaller CI Treatment[4] and the Present Work

property	ref 4	this work
R_e (bohr)	3.622	3.615
R_{max} (bohr)	4.731	4.740
D_{eff} (eV)	0.447	0.514
ω_{01} (cm^{-1})	529	527
no. of v-levels	9	9[a]

[a] Nine bound states from Numerov-Cooley method; ten bound states using wave packet dynamics.

Potential energy curves calculated as described above for the low-lying electronic states of Cl_2^{3+} are shown in Figure 1. These data are expected to be more accurate than those reported previously due to the use of a lower selection threshold, inclusion of more roots, choice of a larger reference space and diagonalization of a larger SAF space. As can be seen, only the ground state is metastable and can support bound vibrational states, although the second excited state $2^2\Pi_u$ is almost metastable.

4.3. *R*-Dependent Transition Moments. The magnitude of the transition moments between the X $^2\Pi_g$, $(1,2,3)^2\Pi_u$, and $1^2\Sigma_u^+$ states is shown in Figure 2. As can be seen, the transition moment to $2^2\Pi_u$ is significant at intermediate distances but later falls off, whereas the transition to $1^2\Pi_u$ is important at all distances and becomes dominant at $R \geq 4$ bohr. This transition, whose moment becomes asymptotically linear in R, corresponds to the charge-transfer excitation $Cl^+\cdots Cl^{2+} \rightarrow Cl^{2+}\cdots Cl^+$. Furthermore, the interaction between X $^2\Pi_g$ and $1^2\Pi_u$ at 800 nm, which is the wavelength used in our experiments, is one-photon-resonant at $R \sim 4$ bohr, close to the equilibrium position of neutral Cl_2. At the same time, the state $2^2\Pi_u$ is nonresonant with the ground state for all relevant R. Finally, transitions to the $^2\Sigma_u^+$ state are weak at all R. Thus, a two-surface model of dissociation which includes the $X^2\Pi_g \rightarrow 1^2\Pi_u$ charge-transfer transition contains the most important elements of a full treatment.

4.4. Field-Dressed Potential Curves. For the field-dressed states, the excited state was lowered by the photon energy $\hbar\omega_L$ corresponding to laser wavelength of 800 nm. The field-dressed structure is shown in Figure 6. The limit of zero off-diagonal element gives the solid curves in Figure 6. Figure 6 also shows the perturbation of the original potential curves as a result of increasing the laser field intensity. At the zero-field limit the curve crossing occurs at 3.85 bohr. This crossing point lies 0.005 hartree above the potential minimum, while the v = 0,1,2 levels lie at 0.0011, 0.0034, and 0.0057 hartree above the minimum. Thus, vibrational states above $v = 1$ can be dissociated via a laser-induced bond-softening mechanism[10] even in the limit of very low fields.

When the field intensity reaches 1×10^{13} W/cm^2 (dash−dotted line, Figure 6) the lower electronic state supports no more

bound vibrational states, so all vibrational levels in this state are dissociative at this intensity and above. Note that the upper electronic state does support many vibrational levels when the laser pulse is on. As soon as the pulse is removed, however, a system in this state will dissociate on its original (repulsive) potential curve. Survival of the population excited to the upper "bond-hardened" state is only possible due to nonadiabatic transfer of population down to the ground state during the pulse turn-off, as will happen in the limit of very short pulses. In the wave packet dynamics to follow, a time delay introduced between pump and probe pulse allows the excited state to decay, so that the dynamics which result are those characteristic of the lower (metastable) potential curve.

5. Approaches to Pump−Probe Spectroscopy of Cl_2^{3+}

We propose two approaches to study spectroscopy of Cl_2^{3+}, both of which are based on pump−probe techniques. Designing a pump−probe scheme for the spectroscopy of trications requires an understanding of the excitation created by an intense pump, which also establishes the requirements for the probe pulse. Clues for such understanding are provided by the experimental data, which were summarized in the previous section. Preliminary experimental data described at the end of this section emphasize the stringent restrictions imposed on the pump and the probe pulses.

Experiments aimed at the spectroscopy of Cl_2^{3+} cannot rely on detailed knowledge of the manifold of electronic excited states. Consequently, details of electronic excitation of Cl_2^{3+} by an intense ultra-short pump pulse, which is expected to occur based on our experiment, are not known. Fortunately, the pump−probe scheme for Cl_2^{3+} relies on the fact that all electronically excited states of Cl_2^{3+} will dissociate after sufficient delay. We performed wave packet calculations for the field-free dynamics on the excited surfaces, which show that a 40 fs delay is sufficient for dissociation of all electronically excited states.

In the first approach, the standard pump−probe scheme would use an ultra-short pump pulse to produce a well-defined vibrational wave packet in Cl_2^{3+} on the ground state surface, and add sufficient delay before the probe to allow for dissociation of all electronically excited states. As is clear from Figure 6, if the wave packet is caught by a short probe in the vicinity of $R \approx 4$ bohr, efficient 1-photon resonant dissociation would follow. A clearly detectable signal would then be a modulation in the number of stable Cl_2^{3+} in the mass spectrum, as a function of the delay between the pump and the probe.

Another possible way to detect the vibrational spectrum of Cl_2^{3+} would be to use a long, chirped probe pulse with very weak intensity. The method is conceptually similar to that used for Rydberg atoms to measure electronic energy levels,[11] where the electric field strength increases linearly with time, inducing sequential ionization of progressively lower states. As the frequency of the laser increases, the position of resonance will move toward the minimum of the ground-state potential (see Figure 6). As the resonance (curve-crossing) passes through the outer turning point of each v-level, there should be selective absorption and successive depopulation of each. This method would allow one to detect discrete vibrational states by the presence of steps in Cl_2^{3+} signal. It would also measure the change in the transition energy between the lower and upper surfaces at the right turning points of successive vibrational levels, providing rather stringent test for the theoretical prediction of the energy gap between the potential energy surfaces.

For an effective realization of the pump−probe scheme based on the first approach we need to understand the following issues. First, it is important to understand how short the pump pulse should be to ensure excitation of a well-localized and well understood vibrational wave packet under the conditions of very high pump intensity.

Second, any pump−probe scheme for trications must take into account the fact that an intense pump pulse creates not only triply-, but also singly- and doubly charged ions. While triply charged ions have only one metastable potential energy surface, singly and doubly charged ions have many stable or metastable surfaces. For example, the presence of many Cl_2^{2+} ions after a 12 fs pulse is unavoidable, and these ions can be both in ground and excited electronic states. The probe pulse can promote these states to Cl_2^{3+}, so that vibrational motion in the lower charge states can potentially contribute to the pump−probe signal in Cl_2^{3+}, even when the probe intensity is insufficient to create Cl_2^{3+} on its own. Therefore, the probe pulse intensity must be kept as low as possible to avoid contamination of the signal due to the creation of Cl_2^{3+} by the probe pulse, e.g., from the excited states of Cl_2^{2+} with low ionization potential. On the other hand, it has to be high enough to induce clearly detectable modulation in the Cl_2^{3+} signal.

Third, 10−20 fs pulses with peak intensity up to 10^{15} W/cm^2 are typically followed by a much weaker and significantly longer tail. In most problems in intense-field physics this tail is unimportant, but for fragile trications the situation is quite different; even a weak field is capable of softening a very weak bond, as is clear from Figure 6.

To gain some quantitative understanding of these three issues, we performed three groups of numerical simulations. To establish the required duration of the pump pulse, we simulated wave packet dynamics in Cl_2^{3+} induced by the pump by making a vertical transition to the ground-state surface of Cl_2^{3+} at the peak of 15 and 30 fs pump pulses, and allowing the wave packet to evolve in Cl_2^{3+} during the second half of the pump. For $\tau = 15$ fs and a peak intensity of 7.5×10^{14} W/cm^2, the populations of different vibrational states after the end of the pulse are approximately the same as Franck−Condon (FC) factors of the Cl_2 onto the Cl_2^{3+} in the field-free case. However, when τ is increased to 30 fs, the populations change dramatically, with a strong decrease of the populations in $v = 0$ and 1, and an increase in the populations of the higher vibrational levels. The final wave packet in this case becomes strongly dependent on pulse parameters and details of (unknown) electronic structure of Cl_2^{3+}. Hence, one should use pump pulses with duration around 10−15 fs or less.

To establish the range of lowest probe intensities for which the modulation in Cl_2^{3+} signal is sufficient for detection, we have performed a different series of numerical simulations. On the basis of the discussion above, a vertical transition to the Cl_2^{3+} ground-state surface was assumed, with the vibrational wave function corresponding to the $v = 0$ vibrational level of Cl_2. Overlap integrals between Cl_2 ($v = 0$) and Cl_2^{3+} ($v = 0-4$) give Franck−Condon (FC) factors 0.174, 0.410, 0.332, 0.081, and 0.001 for $v = 0-4$, respectively. As can be seen from the sum, no other transitions have nonzero FC factors. The vertical transition has a maximum probability into $v = 1$, caused by the fact that the position of the minimum in Cl_2^{3+} is shifted inward by 0.20 bohr relative to Cl_2. The $X^2\Pi_g$ ground state and $1^2\Pi_u$ excited-state potential curves and the transition moment between these states were used as input to the wave packet propagation procedure. The wave packet on the ground state was allowed

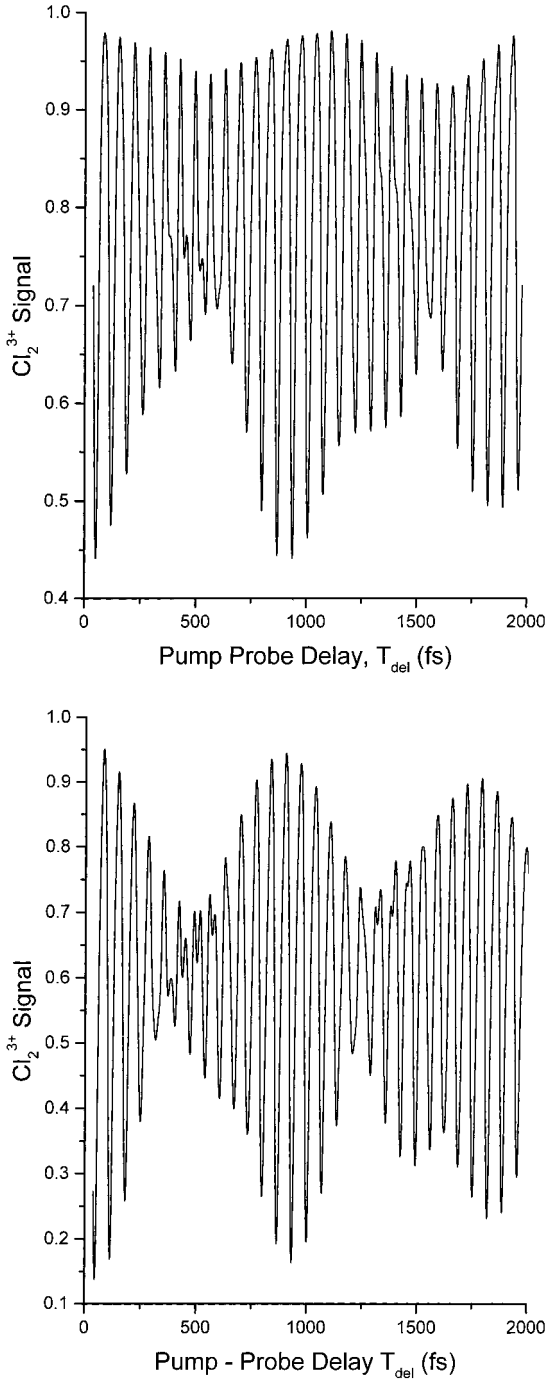

Figure 7. Calculation of Cl_2^{3+} signal as a function of time delay between the pump and the probe for two probe intensities: (a) $I = 7.9 \times 10^{12}$ W/cm^2 and (b) $I = 1.0 \times 10^{14}$ W/cm^2.

to evolve field-free for a delay time T_{del}, where $T_{del} > 40$ fs. Following T_{del}, a sin^2 probe pulse with a central wavelength of 800 nm and a base-to-base duration of 30 fs was initiated. The norm of the wave packet remaining on the ground-state trication potential was then recorded as one data point. The process was repeated for increasing T_{del} up to a total delay time of 2 ps. About 1000 points were used to obtain sufficient resolution of the time-delay signal. Figure 7(a) shows the results of this calculation for a weak probe field of peak intensity 7.9×10^{12} W/cm^2, where the "Cl_2^{3+} signal" refers to the amount of Cl_2^{3+} remaining. This field intensity is just strong enough to dissociate $v = 0$ (see Figure 6). Thus, intensities just below 10^{13} W/cm^2 would represent a practical limit for creating sufficiently large modulation of the Cl_2^{3+} signal.

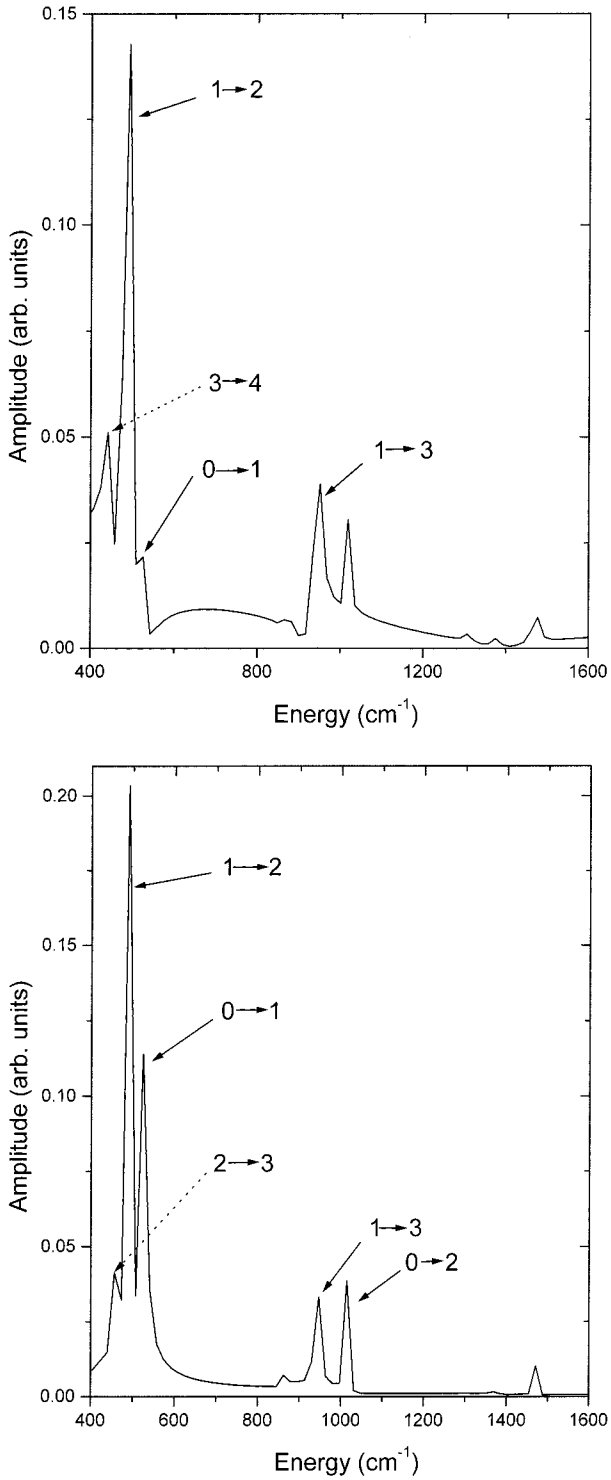

Figure 8. Vibrational spectra of Cl_2^{3+} obtained from the Fourier transform of data in Figure 7: (a) $I = 7.9 \times 10^{12}$ W/cm^2 and (b) $I = 1.0 \times 10^{14}$ W/cm^2.

Figure 7(b) shows another calculation for a stronger probe field of peak intensity 1.0×10^{14} W/cm^2, which can easily dissociate all v-levels. The rephasing of the wave packet is clear in both cases, and this rephasing over 2 ps allows an accurate Fourier transform of the intensity signal from the time domain into the frequency domain.

Frequency-domain spectra resulting from the Fourier transform of Figures 7(a) and (b) are shown in Figures 8(a) and (b), respectively. The Fourier transform of Figure 7(a) indicated two frequencies and traces of a third (shoulder at right of main peak). These frequencies correspond to 0−1 (small peak on right

TABLE 3: Comparison of Vibrational Level Spacings Obtained by Numerov-Cooley Method and FFT for Cl_2^{3+}

transition[a]	Numerov−Cooley	FFT
0−1	527	526
1−2	492	492
2−3	460	459
3−4	439	441

[a] All transitions in cm^{-1}.

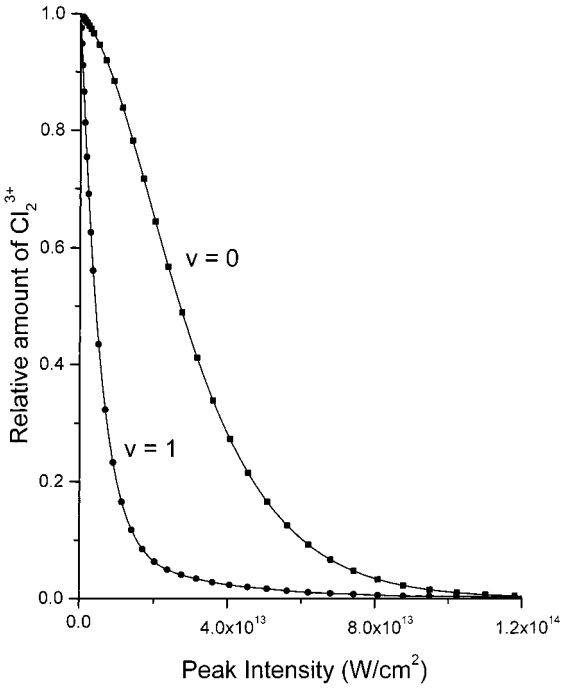

Figure 9. Relative amount of Cl_2^{3+} signal as a function of laser intensity using pure eigenstates as initial conditions.

shoulder of main peak), 1−2 (main peak, 492 ± 5 cm^{-1}), and 3−4 (medium peak on left shoulder of main peak), as well as overtones. Thus, even though 2−3 is obscured by the main peak we were able to locate it at 439 cm^{-1}. Next group of peaks forms the overtone spectrum corresponding to (0−1 + 1−2) = 1018, 1−3 = 951, and (0−1 + 1−2 + 2−3) = 1477 cm^{-1}. To verify the assignment and to look for new peaks, the calculation was repeated at a maximum probe intensity of 1.0×10^{14} W/cm^2 (Figure 8b). Comparison of the lower vibrational level spacings obtained by Numerov-Cooley and wave packet methods for the lower υ-levels is shown in Table 3. Agreement is within 2 cm^{-1} for transitions up to $\upsilon = 4$.

To establish the potential effect of the weak and long tail in the intense short pump, a study was done of the dissociation of the various vibrational levels of the trication in the laser field. The vibrational wave functions of the trication were used as input to the wave packet propagation procedure. Vibrational eigenstates were exposed to a $\sin^2$ pulse which was 130 fs base to base (ca. 50 fs fwhm of a $\sin^4$ envelope) of variable maximum intensity. Figure 9 shows the results up to an intensity of 1.2×10^{14} W/cm^2 for the $\upsilon = 0$ and $\upsilon = 1$ levels. This figure shows that even in a weak field of intensity 4×10^{13} W/cm^2, the $\upsilon = 1$ level of the trication will be almost completely dissociated, whereas $\upsilon = 0$ can survive to higher field strengths. Therefore, all the vibrational levels above $\upsilon = 0$ can easily be dissociated by the tail of the pump pulse, destroying the vibrational wave packet.

Using the apparatus described in the previous section we carried out a prelimenary experiment. We measured the yield of Cl_2^{3+} as a function of the time delay between the pump and the probe pulses. The probe pulse in this case was quite intense, about 20% of the pump ($I_{pump} \sim 10^{15}$ W/cm^2). We observed modulation in the Cl_2^{3+} signal for both positive and negative (probe preceding the pump) time delays with modulation periods of 65 and 55 fs, respectively. It is important to note that no such modulations were observed for a weak probe, $I_{probe} \sim 10^{14}$ W/cm^2, and we did not observe any revivals at longer times.

An explanation of these observations is related to the novel aspects of dealing with an intense pump pulse. The absence of clear modulation for a weak probe is probably caused by the weak but long tail of the intense ultrashort pump pulse, which dissociates excited vibrational states via the bond-softening mechanism. Consequently, the wave packet created by the vertical transition from the neutral is strongly modified, and the population resides mostly in $\upsilon = 0$ of Cl_2^{3+}. Therefore, no clear modulation is present unless the probe itself is intense enough to promote vibrational wave packets created in lower charge states, e.g., Cl_2^{2+}, to the triply charged state. Such a possibility is clear from the experimental results for negative delay times, when the probe that precedes the pump does not produce Cl_2^{3+}.

The fact that the modulation period for negative delay (55 fs) is somewhat different from that for positive delays (65 fs) implies that for positive delays the observed modulation signal should be a mixture of transitions from several electronic surfaces and does not originate solely from the wave packet motion in Cl_2^{3+}. In this case, revival is highly unlikely. Thus, an intense pump pulse creates observational difficulties when trying to measure a vibrational spectrum. To circumvent the difficulty experimentally, one has to compensate for all sources of high-order dispersion introduced into the amplified ultrashort pulse, e.g. at the pulse compression and amplifying stages. This can be done in the Fourier plane, using liquid crystal modulator to adjust the phases of different colors constituting the pump pulse.

As mentioned earlier, another possible way to detect the vibrational spectrum of Cl_2^{3+} would be to use a long, chirped probe pulse with very weak intensity. To see if this effect could be observed, we performed computational experiments on pure eigenstates. We found that a 307 fs weak pulse (8.8×10^{11} W/cm^2) chirped from 8800 to 11 000 cm^{-1} will dissociate 47% of $\upsilon = 3$ but only 5% of $\upsilon = 2$. This means that an experiment to detect vibrational spectra by control of the chirp rate in a laser field is feasible. Such experiments to detect vibrational spectra by controlling the chirp rate are now in progress in our laboratory.

6. Conclusions

This and previous work from the authors[4] has shown that in the laboratory we can generate highly charged ions of chlorine, including the metastable molecular ion Cl_2^{3+}. Some aspects of the production of these ions have been discussed in the present paper. We propose two approaches to study vibrational spectra of Cl_2^{3+}, both of which are based on the femtosecond pump−probe technique. In the first approach, a variable time-delay between the intense pump and the probe pulse was used to observe modulations in the Cl_2^{3+} signal. Theoretical simulations gave an insight into the requirements of the pump and probe pulses. Our preliminary experiment showed modulation of the Cl_2^{3+} signal but this could not be clearly attributed to the vibrational motion. The reason for this is that in pump−probe experiments the chlorine ions will be generated in a variety of

electronic and ionic charge states, not only in the ground state of Cl_2^{3+}. Relative populations of the different charged ions, and the negative time-delay experiments, indicate that ionization from lower charge states result in extra modulation of the signal, which does not originate from wave packet motion in Cl_2^{3+}. The experiment also did not show any revival of the wave packet required to give an accurate vibrational spectrum. Our simulations on accurate potential surfaces have shown that even the relatively weak tail of the intense pump pulse can dissociate higher vibrational states. Thus, generation of a wave packet by vertical excitation from Cl_2 and the resulting FFT deconvolution of time-delay experiments, while valid in principle, faces severe experimental difficulties. Simulations show that if the pump pulse tail is eliminated, a spectrum can be obtained. Ways to reduce the intensity of the pump tail were discussed. A second approach was proposed, which requires chirping of the pump laser pulse, causing the position of the resonance to shift and resulting in a sampling of the different vibrational states. Simulations based on this approach show discrimination of vibrational states. Refined experiments to test these ideas are currently under investigation in our laboratory.

References and Notes

(1) Zewail, A. H. *J. Phys. Chem. A* **2000**, *104*, 5660.
(2) Schröder, D.; Schwarz, H. *J. Phys. Chem A* **1999**, *103*, 7385.
(3) Peyerimhoff, S. D.; Buenker, R. *J. Chem. Phys.* **1981**, *57*, 279.
(4) Wright, J. S.; DiLabio, G. A.; Matusek, D. R.; Corkum, P. B.; Ivanov, M. Yu.; Buenker, R. J.; Alekseyev, A. B.; Hirsch, G. *Phys. Rev. A* **1999**, *59*, 4512.
(5) Buenker, R. J.; Peyerimhoff, S. D.; Butscher, W. *Mol. Phys.* **1978**, *35*, 771; Buenker, R. J.; Phillips, R. A. *J. Mol. Struct.* (*THEOCHEM)* **1985**, *123*, 291.
(6) Cooley, J. W. *Math. Comput.* **1961**, *15*, 363.
(7) See, e.g., Delone N. B.; Krainov V. P. *Atoms in Strong Light Fields*; Springer, Berlin, 1985. George, T. F. *J. Phys. Chem.* **1982**, *86*, 10.
(8) Nisoli, M.; De Silvestri, S.; Svelto, O. *Appl. Phys. Lett.* **1996**, *68*, 2793.
(9) Dietrich, P.; et al. *Phys. Rev. A* **1993**, *47*, 2305.
(10) See, e.g., Bucksbaum, P. H.; Zavriyev, A.; Muller, H. G.; Schumacher, D. W. *Phy. Rev. Lett* **1990**, *64*, 1883. Guisti-Suzor, A.; Mies, F. H.; Dimauro, L. F.; Charron, E.; B.Yang, B. *J. Phys. B* **1995**, *28*, 309.
(11) See, e.g., Gallagher, T. F. *Rydberg Atoms*; Cambridge University Press: 1994.
(12) Sakai, H.; Stapelfeldt, H.; Constant, E.; Ivanov, M. Yu; Matusek, D. R.; Wright, J. S.; Corkum, P. B. *Phys. Rev. Lett.* **1998**, *81*, 2217.
(13) Stapelfeldt, H.; Constant, E.; Corkum, P. B. *Phys. Rev. Lett*. **1995**, *74*, 3780.
(14) Rolland, C.; Corkum, P. B. *J. Opt. Soc. Am. B* **1988**, *5*, 641.